Supplementary Information

# Superspreading-Photoinitiated *In Situ* Construction of Hydrogel Electrolyte Enabling High-Performance and Long-Cycling Zinc-Ion Batteries

Jihao Fan,[12] Linlin Ma,[*12] Ziqiang Zhao,[12] Meng Yu,[12] Yue Wu,[12] Shengwen Kong,[*12] Yanglansen Cui,[*12] Chuangqi Zhao,[*12]

[1]State Key Laboratory of Bioinspired Interfacial Materials Science, School of Chemistry and Materials Science, University of Science and Technology of China, Hefei 230026, China.
[2]Suzhou Institute for Advanced Research, University of Science and Technology of China, Suzhou, 215123, P.R. China.

Corresponding author E-mail: zhaochuangqi@ustc.edu.cn, yanglansen.cui@ustc.edu.cn, malinlin@mail.ustc.edu.cn, kongsw@ustc.edu.cn

**This PDF file includes:**

figures S1 to S16

Table S1

References

**Other Supplementary Materials:**

Movie S1
Superspreading of the pre-polymerization solution on the surface of a superhydrophilic Zn anode

## Experimental Section

### Materials

Acrylamide (AM), 2-Hydroxy-4'-(2-hydroxyethoxy)-2-methylpropiophenone (Irgacure 2959), carboxymethylcellulose Na (CMC), Zn sulfate, Zn acetate and potassium acetate were all purchased from Aladdin, N, N'-methylenebis (acrylamide) (MBAA) was purchased from Macklin. All reagents were used directly without any purification. All zinc foils undergo plasma treatment for 240 seconds prior to use in the oxygen atmosphere.

### Synthesis of SP-CMC-PAM hydrogel electrolyte

A 10 cm×10 cm×0.1 mm Zn anode was plasma treated for 240 s. 3.55 g of acrylamide, 35.5 mg of Irgacure 2959, 7.1 mg of MBAA, 2.5 g of Zn acetate, and 10 g of potassium acetate were dissolved in 5 mL deionized water, and then 10 ml CMC solution of a concentration of 0.0213 g/mL was fully mixed to obtain a pre-polymerization solution. Then, 3 mL pre-polymerization solution was poured on the above Zn anodes, and reacted under UV light (365 nm) irradiation for 3 min to obtain SP-CMC-PAM hydrogel electrolyte synthesized *in situ* on Zn anode. Liquid electrolyte is consisting of 2.5 g of Zn acetate, and 10 g potassium acetate and 15 mL $H_2O$.

### Synthesis of CMC-PAM hydrogel electrolyte

CMC-PAM hydrogel electrolyte was obtained by irradiating the above pre-polymerized solution in a 9 cm diameter PTFE mold with UV light (365 nm) for 3 minutes.

### Preparation of PANi cathode

We prepared the working electrode by adding 0.23 g of ammonium persulfate (APS) to 5 mL HCl solution with the concentration of 1M in a beaker. In another beaker, carbon cloth was immersed in a mixture of 0.36 g aniline and 15 mL HCl solution. Both beakers were cooled at 4 °C. Then, APS solution was added to the aniline mixture to initiate the reaction. After that, the carbon cloth (with polyaniline on it) was removed from the beaker, washed with water and ethanol, and dried at 60 °C for 24 h. The mass loading was approximately 0.5 mg $cm^{-2}$.

### Materials characterization

Scanning electron microscopy (SEM) was conducted using a Quanta S microscope at an accelerating voltage of 20 kV. Attenuated total reflectance Fourier transform infrared (ATR-FTIR) spectroscopy measurements were recorded on an iN10 instrument. All contact angle tests were carried out using a LAUDA Surface Analyzer LSA 100.

### Electrochemical Measurements

CR2032 coin cell was assembled to evaluate the electrochemical performance. In a full-cell system the Zn anode was used as reference and counter electrode. Cyclic voltammogram

(CV) curves were collected at different scan rates (with a voltage range from 0.9 to 1.5 V (vs. $Zn/Zn^{2+}$) in a full-cell system. The electrochemical impedance spectroscopy (EIS) was collected by the CHI760 at the frequency ranging from 0.01 to $10^{-5}$ Hz. Chronoamperometry (CA) testing was conducted in the Zn//Zn symmetrical cell to study diffusion behaviors, with an overpotential of 10 mV. The $t_{Zn^{2+}}$ was obtained by testing EIS before and after CA, and calculated using the following formula[1]:

$$t_{Zn^{2+}} = \frac{I_s * (\Delta V - I_0 R_0)}{I_0 * (\Delta V - I_s R_S)} \quad (1)$$

Meanwhile, the galvanostatic charging and discharging process were used to conduct cycling performance and specific capacity.

**The Calculation of Ionic Conductivity**

The EIS was collected by the CHI760 in the frequency ranging from 0.01 to $10^{-5}$ Hz. The relation between σ and R is calculated according to the following equation[2]:

$$\sigma = \frac{l}{R * S} \quad (2)$$

In this equation, $l$ is the thickness of hydrogel electrolyte, $R$ is the impedence, $S$ is the active area.

**The Calculation of Ion Migration Activation Energy**

The electrochemical impedance spectroscopy (EIS) was collected by the CHI 760 in the frequency ranging from 0.01 to $10^{-5}$ Hz at different temperature. The relation between $E_a$ $and$ $R$ is calculated according to the following equation[3]:

$$\sigma = \frac{A}{T} e^{-\frac{E_a}{RT}} \quad (3)$$

Where $A$ is the pre-exponential factor, $T$ is the temperature, $R$ is gas constant, $E_a$ is ion migration activation energy.

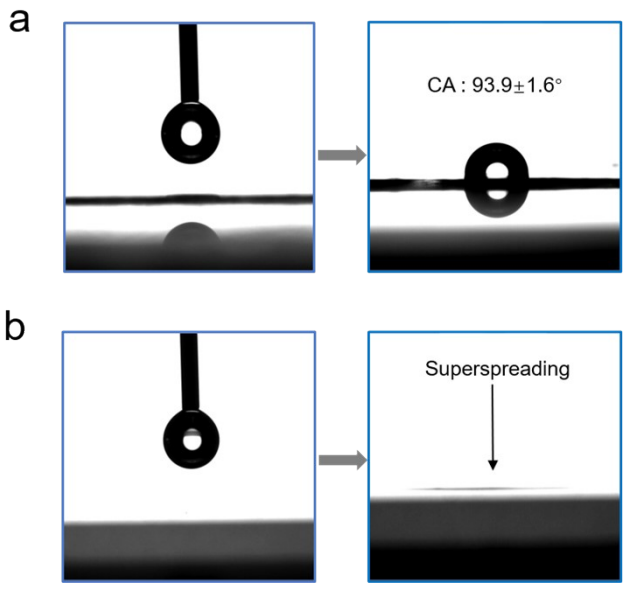


**Figure S1.** Contact angle testing of the reaction solution on the surface of Zn anode. (a) The untreated Zn anode has slight hydrophobicity. (b) The reaction solution can achieve superspreading on the surface of the treated Zn anode.

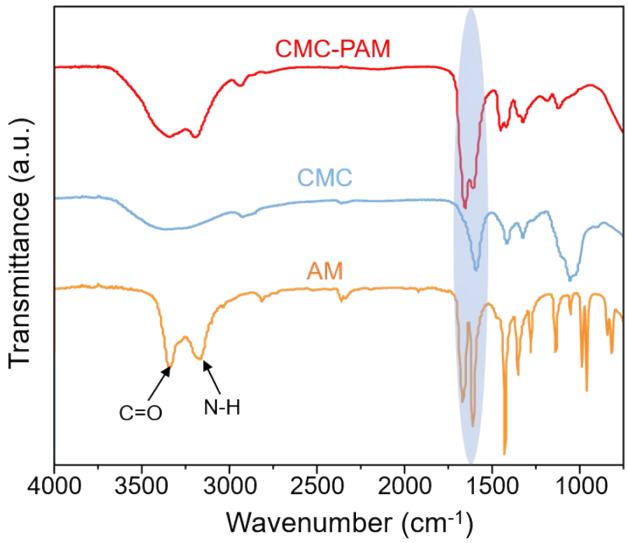


**Figure S2.** FTIR spectra of AM, CMC, and CMC-PAM hydrogel electrolytes.

The FTIR analysis showed that the typical double absorption peaks of AM appeared at 3340 and 3150 $cm^{-1}$, and the characteristic peaks at 1660 and 1610 $cm^{-1}$ could be attributed to C=O stretching vibration and N-H bending vibration. In addition, the FTIR spectrum of CMC shows a characteristic peak of C-O bond at 1050 $cm^{-1}$.

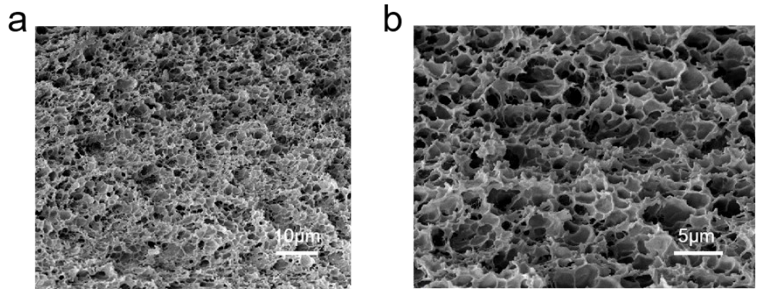


**Figure S3.** (a, b) SEM cross-sectional images of SP-CMC-PAM hydrogel electrolyte at different scales.

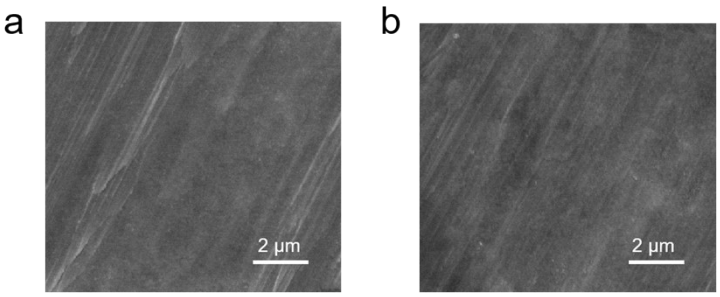


**Figure S4.** The surface morphology of Zn anode before and after plasma treatment.

In order to investigate whether plasma treatment compromises the surface flatness of Zn anodes, the changes in the surface morphology of Zn anodes before and after plasma treatment were observed using SEM. The results showed that the surface morphology of the Zn anode remained almost unchanged before and after plasma treatment.

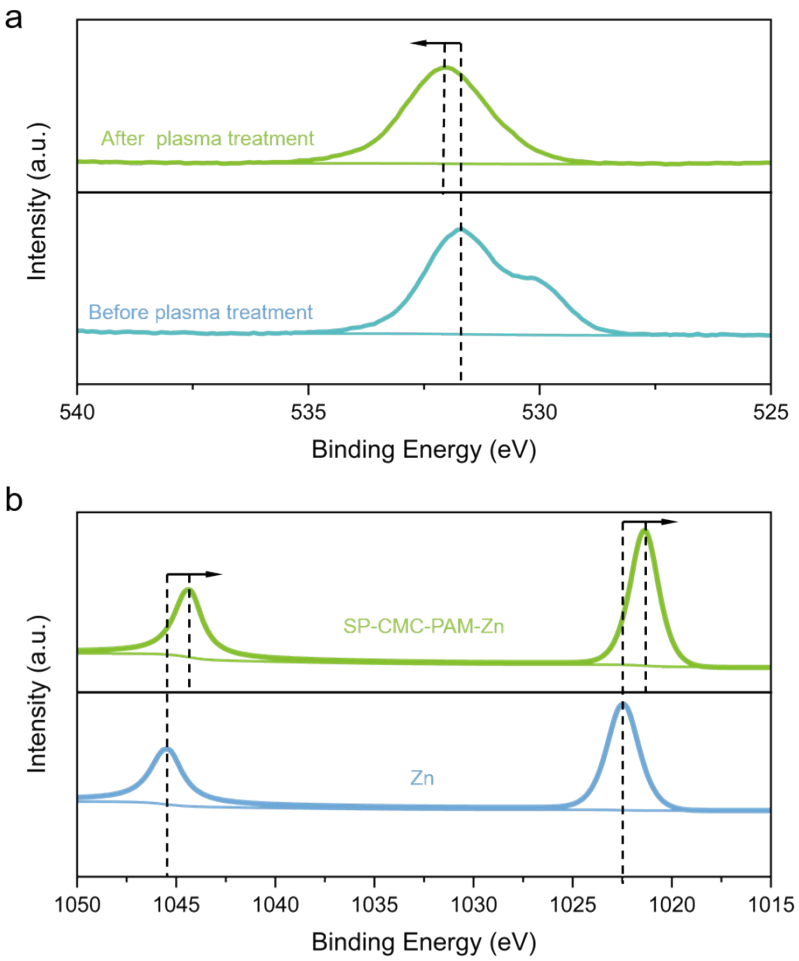


**Figure S5.** High-resolution O 1s and Zn 2p XPS spectra. (a) O 1s XPS spectra of the Zn anode surface before and after plasma treatment. (b) Zn 2p XPS spectra of the Zn anode surface before and after superspreading-photoinitiated *in situ* polymerisation of SP-CMC-PAM.

In Figure S5a, the binding energy of the O 1s peak for the Zn anode shifted from 531.68 ev to 532.08 ev before and after plasma treatment. This confirmed that plasma treatment successfully introduced high oxidation state oxygen-containing functional groups (such as carboxyl groups) onto the zinc surface, thereby enhancing its hydrophilicity. In Figure S5b, the binding energy of the Zn 2p peak for the Zn anode shifted from 1022 ev and 1045 ev to 1021 ev and 1044 ev before and after plasma treatment. The presence of low-valent zinc species at the Zn anode-hydrogel interface strongly indicated the formation of chemical bonds between zinc and functional groups within the hydrogel.

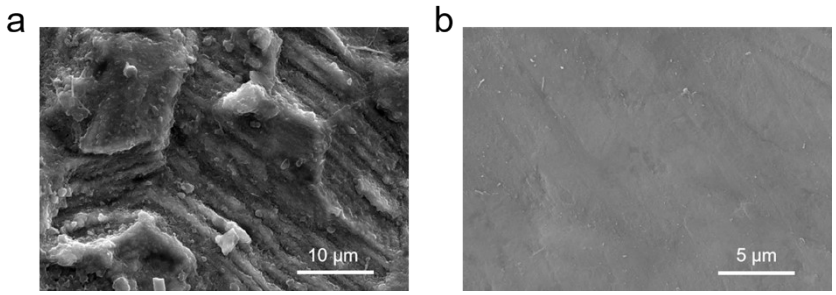


**Figure S6.** The SEM of Zn anode. (a) The SEM of Zn with CMC-PAM hydrogel electrolyte after 100 cycles. (b) The SEM of Zn with SP-CMC-PAM hydrogel electrolyte after 100 cycles.

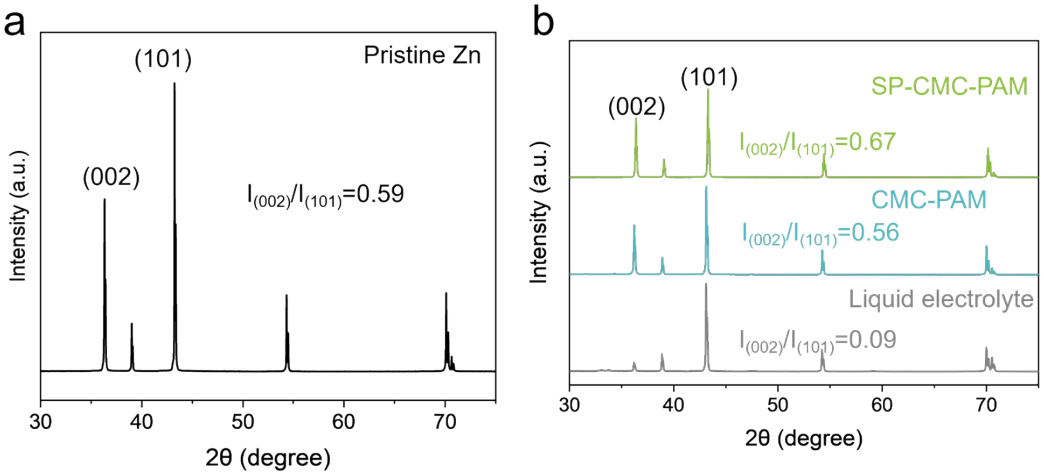


**Figure S7.** (a) XRD pattern of the pristine Zn anode surface and (b) XRD patterns of the deposited state after 50 cycles in Zn//Zn symmetric cells using SP-CMC-PAM hydrogel electrolyte, CMC-PAM hydrogel electrolyte, and liquid electrolyte.

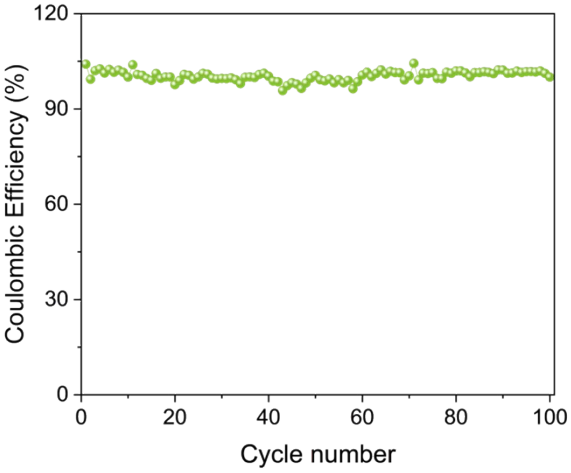


**Figure S8.** The Zn//SP-CMC-PAM//Ti asymmetric cell.

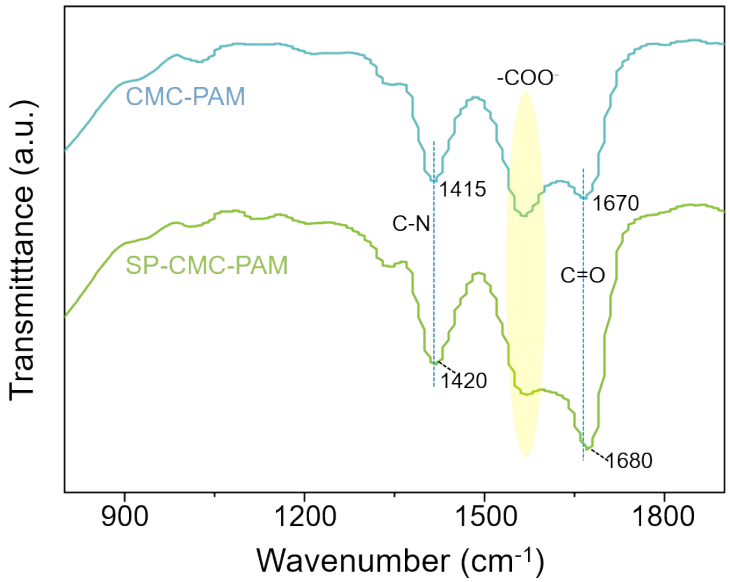


**Figure S9.** FTIR spectra of CMC-PAM and SP-CMC-PAM.

Through comparison of the infrared spectra of *in situ* and *ex situ* gels, it was found that the characteristic FTIR bands for the C=O stretching and C-N stretching of the CMC-PAM amide groups were located at 1415 and 1670 $cm^{-1}$, respectively (the N-H deformation peak was masked by the asymmetric carboxyl peak in CMC). For SP-CMC-PAM, these bands were blue-shifted to higher wavenumbers, particularly at 1420 and 1680 $cm^{-1}$, indicating that during *in situ* polymerization of the hydrogel, Zn forms coordination bonds with CMC-PAM through complexation, enhancing interfacial interactions and thereby improving the ability of CMC-PAM to bind free water.

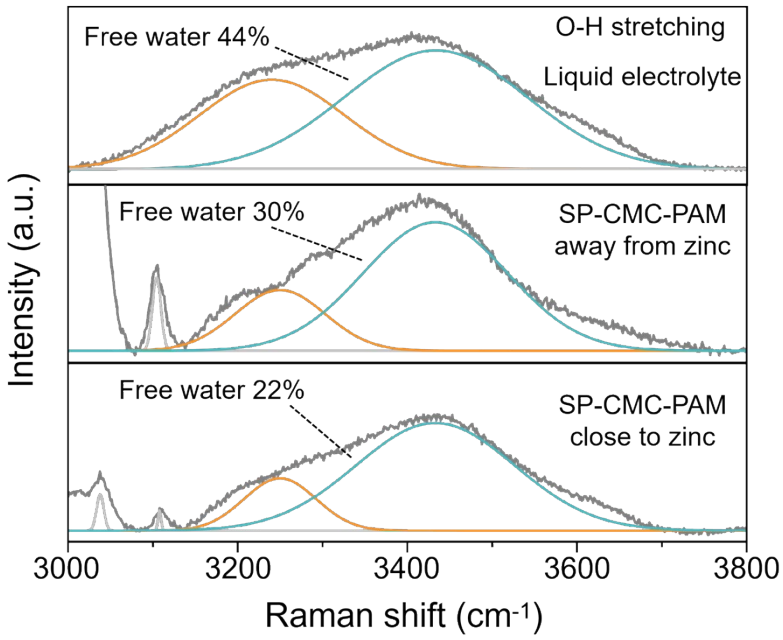


**Figure S10.** Raman spectra show the fitting peaks representing free-water ratio in liquid electrolyte and SP-CMC-PAM away from and close to zinc, respectively.

Raman spectroscopy was employed to identify free water molecules within the hydrogel network. In Raman spectra, peaks around 3200 $cm^{-1}$ are generally assigned to water molecules involved in strong hydrogen bonding, while peaks near 3400 $cm^{-1}$ correspond to water molecules with medium or weak hydrogen bonding.[4] The liquid electrolyte (zinc acetate) exhibited a high free water content (44%), while the free water content in SP-CMC-PAM close to zinc (22%) was lower than that in SP-CMC-PAM away from zinc (30%). This indicated that the polymer network played a crucial role in trapping water molecules, and that coordination bonds and enhanced hydrogen bonding interactions at the electrode-electrolyte interface contribute to locking free water. The free water content at the interface is lower, attributed to the fact that Zn forms coordination bonds with CMC-PAM through complexation, enhancing interfacial interactions and thereby improving the ability of CMC-PAM to bind free water.

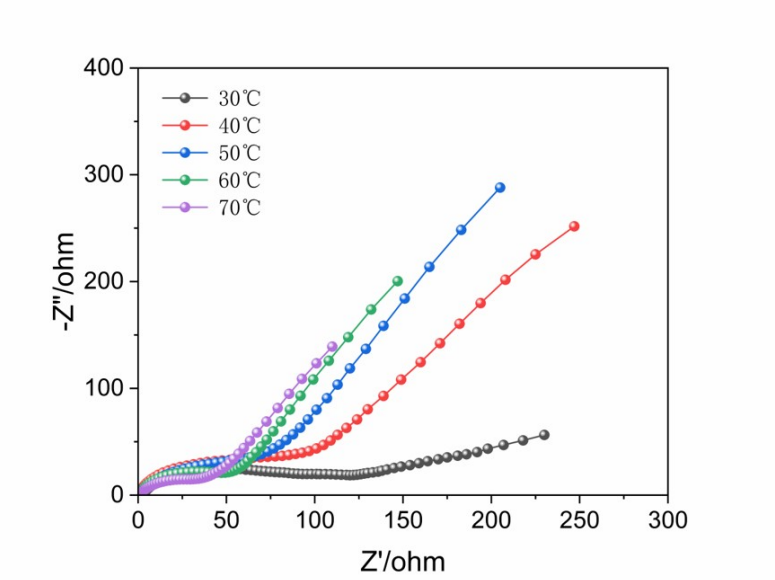


**Figure S11.** Nyquist plots at different temperatures of SP-CMC-PAM hydrogel electrolyte.

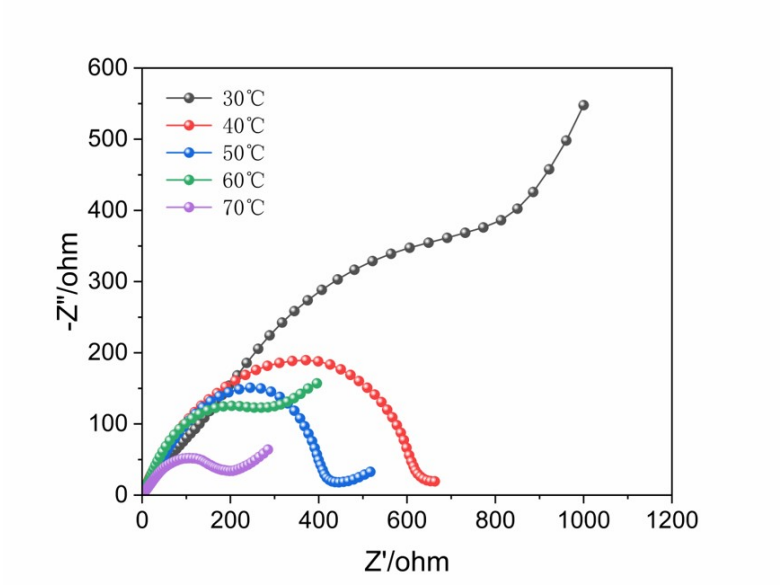


**Figure S12.** Nyquist plots at different temperatures of CMC-PAM hydrogel electrolyte.

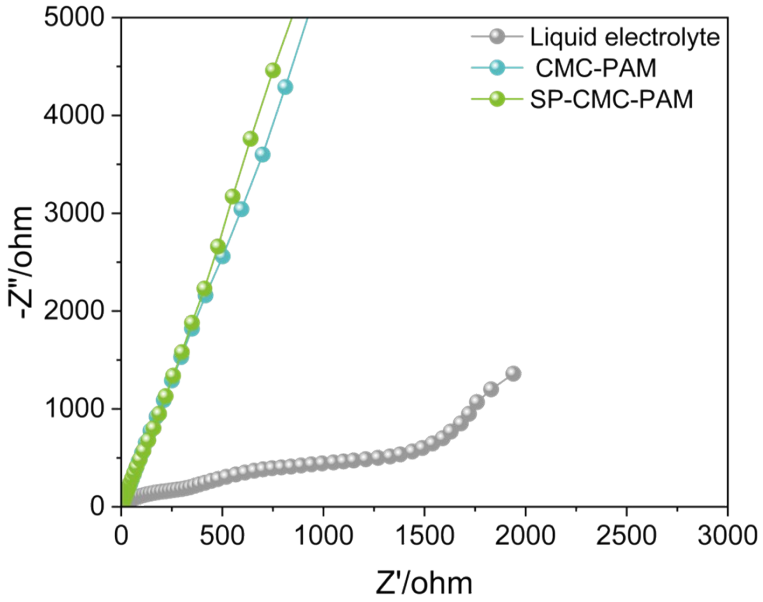


**Figure S13.** Nyquist plots of liquid electrolyte and CMC-PAM and SP-CMC-PAM.

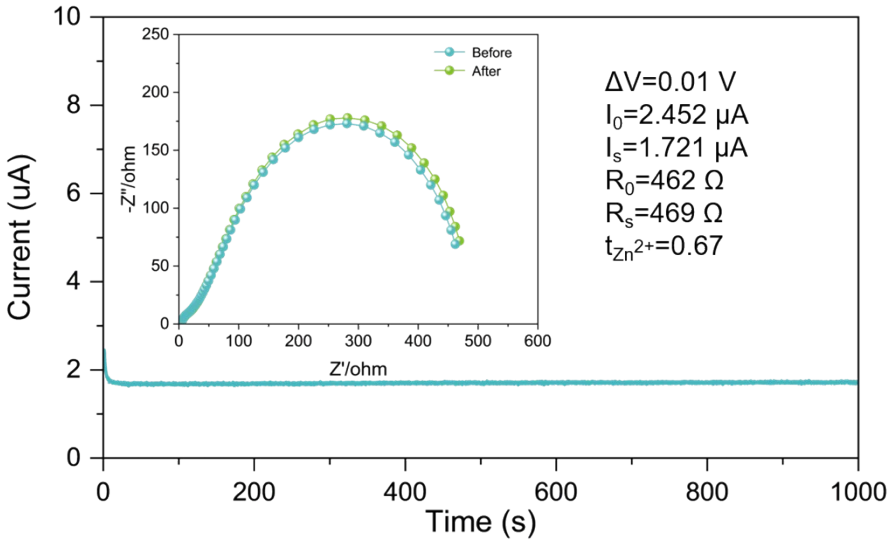


**Figure S14.** The $Zn^{2+}$ transference number of CMC-PAM hydrogel electrolyte.

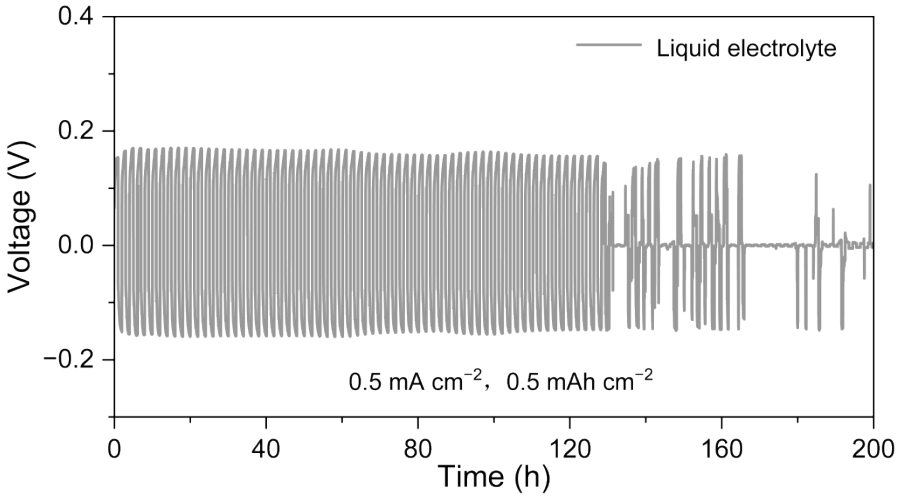


**Figure S15.** Voltage profiles of Zn plating/stripping for Zn//Zn symmetric cells with liquid electrolyte at 0.5 mA $cm^{-2}$/0.5 mAh $cm^{-2}$.

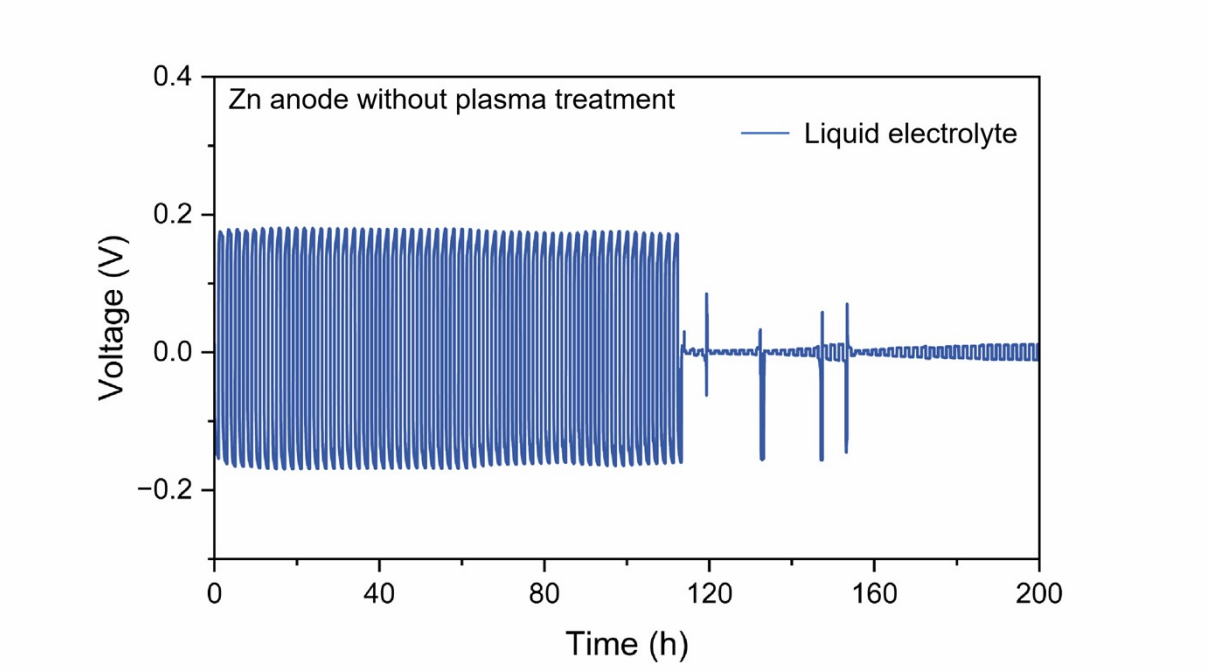


**Figure S16.** Voltage profiles of Zn plating/stripping for Zn//Zn symmetric cells with liquid electrolyte at 0.5 mA $cm^{-2}$/0.5 mAh $cm^{-2}$ (the Zn anode without plasma treatment).

To investigate the effect of plasma-treated zinc anodes on the electrochemical performance of zinc-ion batteries, we compared the cycling performance of symmetric batteries assembled with and without plasma-treated zinc anodes (using liquid electrolytes). The results demonstrated that plasma treatment did not significantly improve the cycling performance of the symmetric batteries (Figures S15, S16).

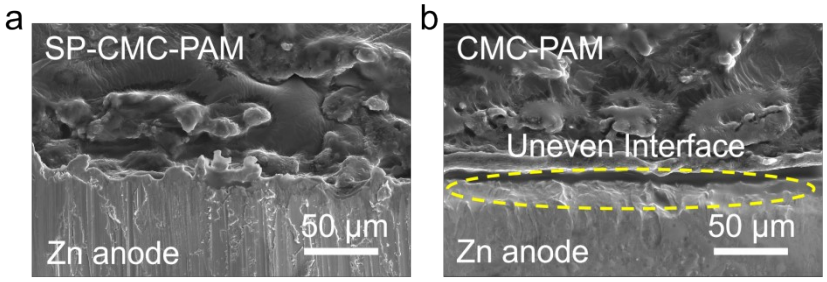


**Figure S17.** SEM images of GPEs/Zn anode interface for SP-CMC-PAM and CMC-PAM after long recycling.

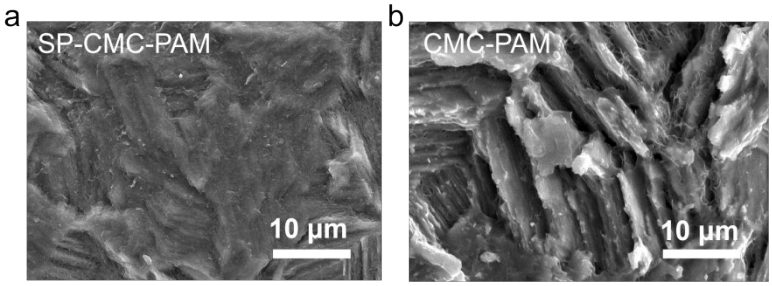


**Figure S18.** (a) The SEM of the Zn anode's surface after 2400 h recycling with (a) SP-CMC-PAM hydrogel electrolyte and(b) CMC-PAM hydrogel electrolyte.

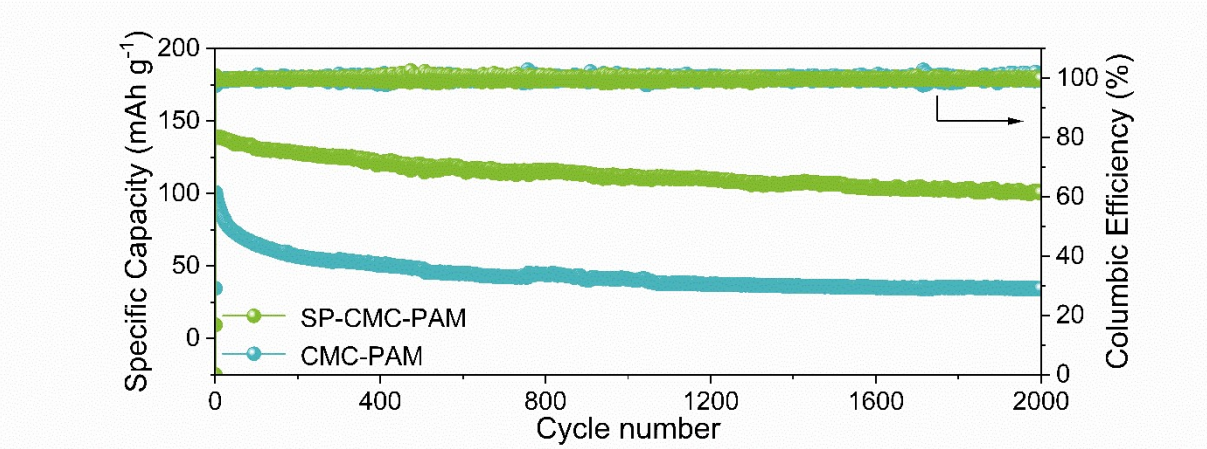


**Figure S19.** Cycling performance of Zn/SP-CMC-PAM/PANi and Zn/CMC-PAM/PANi full batteries at 0.5 A $g^{-1}$, 25 °C, active material loading of 0.5 mg $cm^{-2}$.

**Table S1.** The comparison of various electrochemical properties with reported GPEs.

| Materials | Current density (mA $cm^{-2}$) | Areal capacity (mAh $cm^{-2}$) | Life time (h) | Coulomb efficiency (%) | Ion conductivity (mS $cm^{-1}$) | $t_{Zn^{2+}}$ | Capacity retention (%) |
|---|---|---|---|---|---|---|---|
| **This work** | **0.5** | **0.5** | **2400** | **99.7** | **23.6** | **0.83** | **91** |
| $Zn^{2+}$-CS/PAAM[5] | 0.5 | 0.5 | 375 | 99.1 | 11.6 | 0.85 | 94.6 |
| PVA/$Zn(CF_3SO_3)_2$[6] | 0.1 | 0.1 | 800 | 99.8 | 12.6 | 0.73 | 91.9 |
| ZSC[7] | 0.5 | 0.5 | 200 | 99.5 | 24.6 | 0.79 | 90.4 |
| PVA-D-ES[8] | 1 | 1 | 1200 | 99.2 | 5.68 | 0.78 | 87.3 |
| PZB-931[9] | 0.2 | 0.1 | 2500 | 99.8 | 3.41 | 0.68 | 90 |

**References**


1 J. Cong, X. Shen, Z. Wen, X. Wang, L. Peng, J. Zeng, J. Zhao, Energy Storage Mater., 2021, 35, 586-594.

2 M. Sun, G. Ji, M. Li, J. Zheng, Adv. Funct. Mater., 2024, 34, 2402004.

3 H. Zhang, X. Gan, Z. Song, J. Zhou, Angew. Chem., Int. Ed., 2023, 62, e202217833.

4 T. Zheng, Z. Ju, A.C. Marschilok, E.S. Takeuchi, K.J. Takeuchi, G. Yu, Proc. Natl. Acad. Sci., 2026, 123, e2525975123.

5 Y. Liu, A. Gao, J. Hao, X. Li, J. Ling, F. Yi, Q. Li, D. Shu, Chem. Eng. J., 2023, 452, 139605.

6 S. Huang, F. Wan, S. Bi, J. Zhu, Z. Niu, J. Chen, Angew. Chem. Int. Ed., 2019, 58, 4313.

7 F. Mo, Z. Chen, G. Liang, D. Wang, Y. Zhao, H. Li, B. Dong, C. Zhi, Adv. Energy Mater., 2020, 10, 2000035.

8 J. Kang, Z. Jiang, L. Wen, Adv. Funct. Mater., 2025, 2422566.

9 M. Wang, A. Emre, S. Tung, A. Gerber, D. Wang, Y. Huang, V. Cecen, N. A. Kotov, ACS Nano, 2019, 13, 1107.